Engineering 3 (2017) 452–459

Contents lists available at ScienceDirect

Engineering

journal homepage: www.elsevier.com/locate/eng

Research
Clean Energy—Review

Review on Alkali Element Doping in Cu(In,Ga)Se_2 Thin Films and Solar Cells

Yun Sun [a,*], Shuping Lin [a], Wei Li [b], Shiqing Cheng [a], Yunxiang Zhang [a], Yiming Liu [c], Wei Liu [a]

[a] Tianjin Key Laboratory of Thin Film Devices and Technology, College of Electronic Information and Optical Engineering, Nankai University, Tianjin 300071, China
[b] Engineering Research Center of Nano-Structured Thin Film Solar Cell, Beijing 102211, China
[c] Mads Clausen Institute, University of Southern Denmark, Sønderborg 6400, Denmark

ARTICLE INFO

Article history:
Received 3 May 2017
Revised 2 July 2017
Accepted 9 July 2017
Available online 25 August 2017

Keywords:
Alkali elements
Cu(In,Ga)Se_2
Thin-film solar cells
Post-deposition treatment

ABSTRACT

This paper reviews the development history of alkali element doping on Cu(In,Ga)Se_2 (CIGS) solar cells and summarizes important achievements that have been made in this field. The influences of incorporation strategies on CIGS absorbers and device performances are also reviewed. By analyzing CIGS surface structure and electronic property variation induced by alkali fluoride (NaF and KF) post-deposition treatment (PDT), we discuss and interpret the following issues: ① The delamination of CIGS thin films induced by Na incorporation facilitates $CuInSe_2$ formation and inhibits Ga during low-temperature co-evaporation processes. ② The mechanisms of carrier density increase due to defect passivation by Na at grain boundaries and the surface. ③ A thinner buffer layer improves the short-circuit current without open-circuit voltage loss. This is attributed not only to better buffer layer coverage in the early stage of the chemical bath deposition process, but also to higher donor defect (Cd^{+}_{Cu}) density, which is transferred from the acceptor defect (V_{Cu}) and strengthens the buried homojunction. ④ The KF-PDT-induced lower valence band maximum at the absorber surface reduces the recombination at the absorber/buffer interface, which improves the open-circuit voltage and the fill factor of solar cells.

1. Introduction

In 2013, Chirilă et al. [1] of the Swiss Federal Laboratories for Materials Science and Technology (Empa) achieved an energy conversion efficiency of 20.4% on a polyimide (PI)-substrate-based Cu(In,Ga)Se_2 (CIGS) solar cell by alkali fluoride (NaF and KF) post-deposition treatment (PDT), which is excellent progress for CIGS-based solar cells. This world-record-setting device, fabricated by the low substrate temperature process, was not only the most efficient CIGS-based solar cell, but also equaled the champion cell efficiency of polycrystalline silicon-based solar cells. As researchers continued to study the PDT process, several institutes rapidly boosted the best device efficiency. In the past three years, the efficiency increments that have been achieved are even larger than those made during the prior 15 years, thus establishing a milestone in progress. In June 2016, Jackson et al. [2] of the Center for Solar Energy and Hydrogen Research Baden-Württemberg (ZSW) set the current world record for efficiency for CIGS-based solar cells, of up to 22.6%, by using heavy alkali element fluoride RbF-PDT treatment.

In 1993, Hedström et al. [3] found that the crystalline structure and device performance of CIGS absorber developed on soda lime glass (SLG) substrate is significantly better than that developed on borosilicate glass. The reason for this phenomenon is the incorporation of sodium (Na), which increases the open-circuit voltage (V_{OC}) and the fill factor (FF), and therefore increases device efficiency [4]. In 1994, Holz et al. [5] revealed that no matter whether the Na was diffused from SLG or introduced by other methods, the material conductivity increased only when the atom density of Na approached 10^{15} cm^{-3}. In 1997, Granata et al. [6] suggested that the device performance deteriorated as the Na concentration approached 1 at%.

* Corresponding author.
E-mail address: suny@nankai.edu.cn

http://dx.doi.org/10.1016/J.ENG.2017.04.020

The optimal concentration was in the range of 0.05 at% to 0.5 at%. In the same year, Contreras et al. [7] from the National Renewable Energy Laboratory unprecedentedly investigated doping with other alkali elements, and revealed that potassium (K) and cesium (Cs) also improved the device V_{OC}, but that Na improved it the most. In 2005, Rudmann et al. [8] from Empa improved the efficiency of CIGS devices on PI substrates up to 14.1% by doping Na on absorbers with PDT treatment. In 2013, as mentioned earlier, Chirilă et al. [1] from Empa demonstrated that the KF-PDT process could improve the conversion efficiency of flexible CIGS devices on a PI substrate to 20.4%.

It is commonly agreed that alkali element doping passivates the defects at the p-type CIGS absorber surface or at grain boundaries. It does not change the acceptor concentration, but decreases the compensating donor concentration [9]. As the free carrier density is determined by the difference in acceptor and donor concentration, the p-type carrier concentration increases; as a result, the Fermi level (E_F) is lowered. Thus, an enlarged E_F differential will produce higher V_{OC} and FF. In this article, we summarize some outcomes achieved by alkali incorporation, such as surface chemical composition and electronic structure variations, and analyze the reasons behind the boost to CIGS-based solar cell efficiency by the induction of alkali PDT.

2. Influences of incorporation strategies on Cu(In,Ga)Se_2 absorbers

There are three commonly adopted alkali incorporation methods: pre-deposition, co-evaporation, and post-deposition. Pre-deposition means that the alkali element diffuses from an alkali-containing substrate. Co-evaporation means that the alkali element is evaporated during the absorber deposition. Post-deposition means that the absorber is deposited first and then annealed with the alkali element (also called the PDT method).

2.1. Pre-deposition incorporation

It is commonly recognized that diffusing Na from the SLG substrate during CIGS evaporation, without intentional incorporation, is a good Na doping method. However, for large-scale SLG, the Na content uniformity is insufficient and deteriorates the module efficiency. The solution is to deposit a thin layer of aluminum oxide (Al_2O_3) or silicon nitride (Si_3N_4) on SLG to prevent elements in SLG from diffusing into deposited CIGS absorbers. Next, Na is distributed uniformly via a method such as sputtering a Na-containing molybdenum (Mo) (MoNa) back contact, which acts as a Na source. Another method is to deposit a NaF layer (NaF precursor), with a certain amount on the Mo back contact to ensure a sufficient supply of Na during the absorber deposition. NaF is stable, and the residual fluorine ion (F^-) reacts with selenium (Se) to form vaporous SeF_6 that can desorb from the absorber [10]. The Na doping is controlled by the NaF layer thickness. Insufficient NaF amount results in low V_{OC} and FF, and an excess amount leads to peeling-off problems during absorber deposition. Moreover, an excess amount of NaF also deteriorates the solar cell performance [11]. Due to the good controllability of the NaF precursor, this method has been commonly adopted.

Salomé et al. [12] compared the performance of CIGS-based solar cells prepared with different Na supply methods, including using SLG, NaF precursor, and a MoNa layer. According to Table 1[12] (where cell parameters are mean values), Sample 3, which is a Na-free device, shows the lowest V_{OC} and FF. Thus, the average conversion efficiency is only 8.8%. Of the rest of the samples with pre-deposition incorporation methods, the NaF precursor sample (Sample 4) shows the best performance, with a significantly higher V_{OC} and FF than the other devices. The second-best performer is the SLG sample (Sample 1), and the worst device among the Na-doped samples is the sample with the MoNa structure (Sample 5). This sample is doped with Na diffused from the Mo back contact layer. The lowest device parameters indicate the lowest doping content. In addition, Sample 2, which was prepared with a MoNa layer on SLG, shows inferior performance compared with Sample 1. We deduce that the MoNa layer blocks the diffusion of Na from SLG to the absorber.

2.2. Co-evaporation incorporation

In 2010, Güttler et al. [13] prepared CIGS absorbers on PI substrate using the three-stage co-evaporation process, and incorporated Na by co-evaporation during the first, second, and third stages, respectively. They compared the film structures with Na-free CIGS film (Fig. 1) [13].

The scanning electron microscope cross-sections in Fig. 1 show that incorporating Na during the first and second stages deteriorates the CIGS crystallinity. Fine grains were found at the film surface and back interface. However, incorporation at the third stage only slightly affects the crystallinity at the film surface, and the corresponding solar cell shows the best performance. The Na-free sample shows larger grain sizes with no stratification. By analyzing the secondary ion mass spectrum (SIMS) profiles (Fig. 2) and comparing the results with Fig. 1, we deduced that gallium (Ga) accumulates at the Cu(In,Ga)Se_2 (CIGS)/Mo interface if Na is incorporated at the first or second stage. These fine grains were composed of high-Ga-content CIGS or $CuGaSe_2$ (CGS). For the samples in which Na co-evaporated at the third stage, fine grains were located at the film surface, and

Table 1
Effects of different Na incorporation methods on the performance of CIGS solar cells [12].

Sample	Substrate	Back contact	Temperature (°C)	V_{OC} (mV)	J_{SC} (mA·cm^{-2})	FF (%)	Conversion efficiency (%)
1	SLG	Mo	540	678 (674–681)	32.48 (32.29–32.68)	76.0 (72.6–77.0)	16.8 (15.8–17.1)
2	SLG	MoNa/Mo	540	625 (605–634)	32.32 (31.93–32.81)	71.0 (63.8–72.2)	14.4 (12.9–15.1)
3	Al_2O_3	Mo	540	480 (393–492)	31.46 (29.15–32.17)	57.8 (38.6–58.7)	8.8 (4.7–9.1)
4	Al_2O_3	Mo/NaF	540	698 (684–703)	32.23 (32.02–32.64)	76.4 (74.9–77.5)	17.1 (16.8–17.5)
5	Al_2O_3	MoNa/Mo	540	590 (577–601)	32.42 (32.13–32.72)	70.0 (67.2–72.7)	13.4 (12.6–14.0)
6	Al_2O_3	MoNa/Mo	600	520 (507–529)	32.55 (32.32–32.78)	65.1 (61.5–67.3)	11.0 (10.1–11.3)
7	Al_2O_3	MoNa/Mo	640	556 (525–574)	32.53 (31.79–32.77)	65.2 (63.3–69.1)	11.8 (10.8–12.7)

J_{SC}: the short-circuit current density.

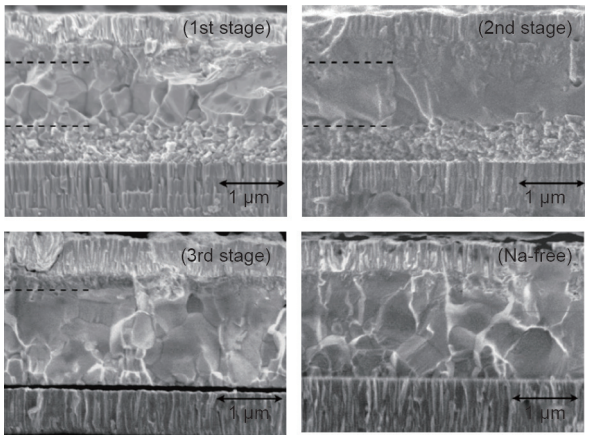

Fig. 1. The effects of Na doping on CIGS film structures during three-stage evaporation [13].

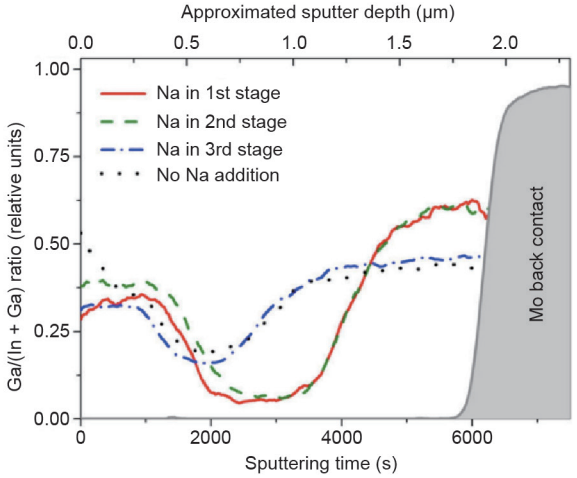

Fig. 2. The effects of Na doping on Ga gradients in CIGS films during three-stage evaporation.

the Ga gradient was similar to that of Na-free samples.

It is now commonly accepted that Na decreases the interdiffusion of indium (In) and Ga, and results in the stratification of CIGS films. In order to understand how Na influences the interdiffusion of In and Ga, Brummer et al. [14] studied the phase transformation during the selenization of Cu/In/Se stack precursors with and without Na by high-temperature X-ray diffraction (HTXRD). It was found that without Na, the $Cu_{2-x}Se$ phase could be detected until the substrate temperature rose to 275 °C. However, with Na, the detectable temperature decreased to 225 °C. This phenomenon proves that Na facilitates the formation of $Cu_{2-x}Se$ at lower temperatures. Therefore, we can deduce that whatever NaF is deposited in the first or second stage facilitates the formation of $Cu_{2-x}Se$. Consequently, as In_2Se_3 is preferred to react with $Cu_{2-x}Se$, the formation of $CuInSe_2$ (CIS) is preferable to the formation of $CuGaSe_2$. The residual Ga_2Se_3 is left at the Mo/CIGS interface and forms small grains. This is the fundamental cause of the film stratification, which is not due to the decreasing interdiffusion of In and Ga. In the three-stage co-evaporation process, after the Cu/Se co-evaporation at the second stage, CIGS and $Cu_{2-x}Se$ both exist in the films. In the third stage, NaF facilitates the formation of CIS, and Ga will still be left at the edge of the films. That is why fine grains are located on the film surface at the third stage. As the layer deposited at the third stage is only a small fraction of the whole film, the fine grain layer is quite thin. The whole film structure is similar to that of the Na-free sample.

We have developed CIGS absorbers on PI/Mo substrate, and incorporated Na during the first, second, and third stages, respectively. The film structures were quite similar to those in Fig. 1. All the film carrier densities increased by 1–2 orders of magnitude compared with the Na-free samples. Thus, the film sheet resistivity decreased by 1–2 orders of magnitude (Fig. 3). The sample with co-evaporated NaF at the third stage showed the best performance; this is because Na has little influence on crystallinity, but rather passivates defects at the film surface or grain boundaries. Excellent crystallinity and passivated surface and grain boundaries are positive factors for higher free carrier concentration.

2.3. Post-deposition incorporation

PDT, which involves the incorporation of alkali elements (Na, K, Rb, Cs) into the CIGS layer under the Se atmosphere after absorber growth, has a wide tolerance for doping level. The PDT process passivates defects without affecting crystallinity; therefore, it improves the electrical properties of CIGS-based solar cells. The substrate temperature for alkali PDT is very important. We have studied CIGS films with NaF-PDT at different substrate temperatures, as shown in Fig. 4. It was found that the sheet resistivity decreased and the carrier concentration improved as the substrate temperature increased. The carrier concentration was saturated at two regions: 250–350 °C and 400–450 °C. From 350 °C to 400 °C, the carrier concentration increased and the resistivity decreased correspondingly. Therefore, a substrate temperature of around 400 °C is commonly adopted for NaF-PDT. In the literature, a substrate temperature between 350 °C and 400 °C is chosen for alkali PDT.

Chirilă et al. [1] fabricated CIGS absorber layers on PI films by co-evaporation; the corresponding solar cell achieved 20.4% conversion efficiency. X-ray photoelectron spectroscopy (XPS) measurement revealed that the surface composition of the CIGS absorber

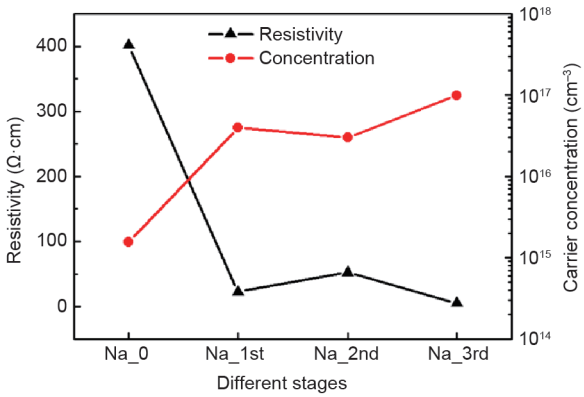

Fig. 3. The effects of Na doping on the electrical properties of CIGS films during three-stage evaporation.

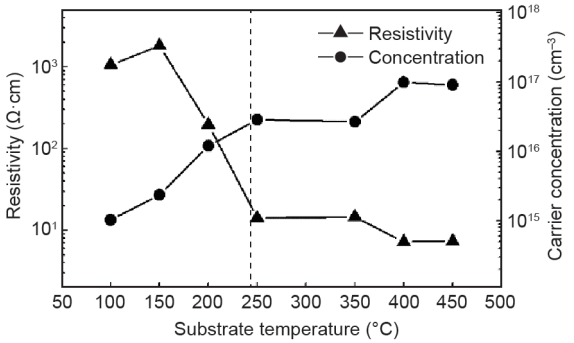

Fig. 4. The thin-film electrical properties after NaF-PDT at different substrate temperatures.

changed with (NaF + KF)-PDT: The Ga concentration decreased obviously and copper (Cu) was depleted. The depletion depth of Cu and Ga was less than 30 nm at the CIGS surface. The fact that the majority of Na was substituted by K indicated that K was preferred to Na to exist in the film.

2.4. Effects of (NaF + KF)-PDT on CIGS device characteristics

Researchers from ZSW improved their solar cell performance significantly by using KF-PDT (Table 2) [2]. The diode quality factor decreased by 12%, the reverse saturation current density (J_0) decreased by about one order of magnitude, the solar cell efficiency improved by 6.9%, the V_{OC} approached 750 mV, and the FF reached over 79%.

As shown in Table 3 [15], compared with the champion cell made in 2013, the new champion cell made in 2014 is improved in every parameter: The J_{SC} is improved by 4.9%, and the corresponding external quantum efficiency (EQE) is obviously increased between the wavelengths of 400–520 nm (Fig. 5(a)) [15]. These variations are mainly attributed to the improvement in the CIGS absorber quality by (NaF + KF)-PDT. The CdS buffer layer is thinner but denser, so the short wavelength absorption is better and the J_{SC} has increased. In addition, the cell made in 2014 clearly presents a steeper Ga gradient and a smaller bandgap minimum than the cell made in 2013, according to the SIMS profiles (Fig. 5(b)). Thus, the EQE of the champion solar cell fabricated in 2014 increased significantly in the range over 1000 nm compared with its predecessor, which is another reason for the increase of J_{SC}. Although such a steep Ga gradient may bring in more lattice defects, however, the V_{OC} or the FF does not decrease compared with the previous champion cell, and the J_{SC} is even able to increase because the minimum bandgap is decreased. It can be deduced that the PDT process passivated the structure defects caused by the steeper Ga gradient. From Table 2 [2], we can see that the shunt resistance, R_{sh}, as well as the J_0 of the solar cells were both significantly optimized. This indicates that the alkali PDT significantly reduced defects at the heterojunction.

2.5. Effects of heavy alkali elements (Rb and Cs) on output characteristics of CIGS-based solar cells

In July 2016, ZSW announced that a CIGS-PDT using the heavy alkali elements rubidium (Rb) and Cs, instead of K, had increased the solar cell efficiency to 22.6%, thereby creating a new world record [2]. The efficiency of solar cells with heavy alkali PDT increased by 6.78% on average, an improvement that was mainly attributed to the increased V_{OC} and FF, as shown in Fig. 6 [2] (without antireflection coating). The average efficiency of solar cells with (Rb or Cs)-PDT is 2.42% higher than that of KF-PDT solar cells. The primary cause is the reduced diode quality factors (Fig. 7) [2]; that is, the diode characteristic of the cells is improved. This indicates that the heavier alkali elements are more effective than K in promoting cell efficiency.

Our team has also started research on the incorporation of heavy alkali elements. Here, we present part of our recent results. We developed four CIGS absorbers in a single run in order to maintain the uniformity of the experimental conditions. Three of the absorbers were post-deposition and were treated with different CsF contents. The last absorber, without any PDT treatment, served as a reference. The doping level was determined by the evaporation temperatures of the CsF. In this study, these temperatures were 320 °C, 290 °C, and 260 °C, respectively. The other experimental conditions were kept the same. As shown in Table 4, the samples with CsF-PDT show a clearly higher V_{OC} and FF; meanwhile, the J_{SC} shows little change because the thickness of CdS is not optimized. As shown in Fig. 8, the doping level of CsF plays a significant role in improving the V_{OC} and FF, and thus in improving the conversion efficiency.

To analyze the cross-section composition, Jackson et al. [2] measured the CsF-PDT samples by SIMS (Fig. 9). It was observed that the

Table 2
A comparison of CIGS cells with PDT (September 2014) and without PDT (January 2011) from ZSW [2].

Date made public	Conversion efficiency (%)	V_{OC} (mV)	J_{SC} (mA·cm^{-2})	FF (%)	CGI	GGI	R_s (Ω·cm^2)	R_{sh} (kΩ·cm^2)	J_0 (A·cm^{-2})	A	J_{PH} (A·cm^{-2})
September 2014	21.7	748	36.5	79.4	0.90	0.32	0.30	1.54	2.2×10^{-11}	1.38	36.5
January 2011	20.3	740	35.4	77.5	0.88	0.34	0.07	0.76	3.8×10^{-10}	1.57	35.6

CGI: atom ratio of Cu/(Ga + In) in absorber; GGI: atom ratio of Ga/(Ga + In) in absorber; R_s: series resistance; R_{sh}: shunt resistance; J_0: reverse saturation current density; A: diode quality factor; J_{PH}: photo-generated current density.

Table 3
A comparison of two CIGS cells from ZSW [15].

Date	Conversion efficiency (%)	J_{SC} (mA·cm^{-2})
2013	20.8	34.8
2014	21.7	36.5

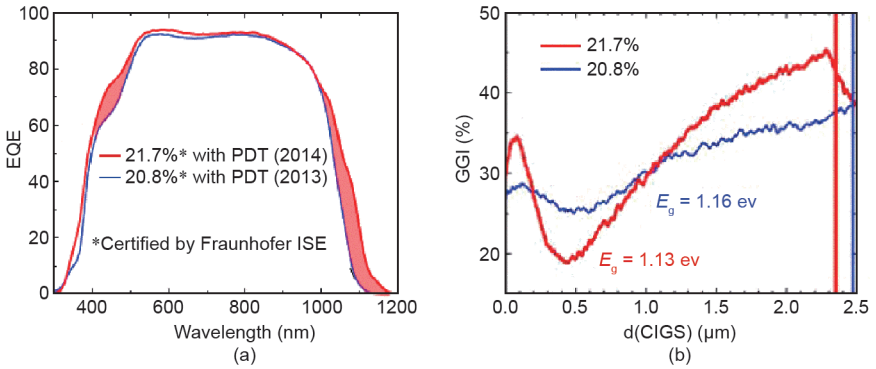

Fig. 5. (a) EQE comparison of two CIGS cells [15]; (b) the atom ratio of Ga/(Ga + In) (GGI) distributions of two CIGS cells characterized by SIMS. d(CIGS): approximated sputter depth of CIGS; E_g: the minimum bandgap of absorber.

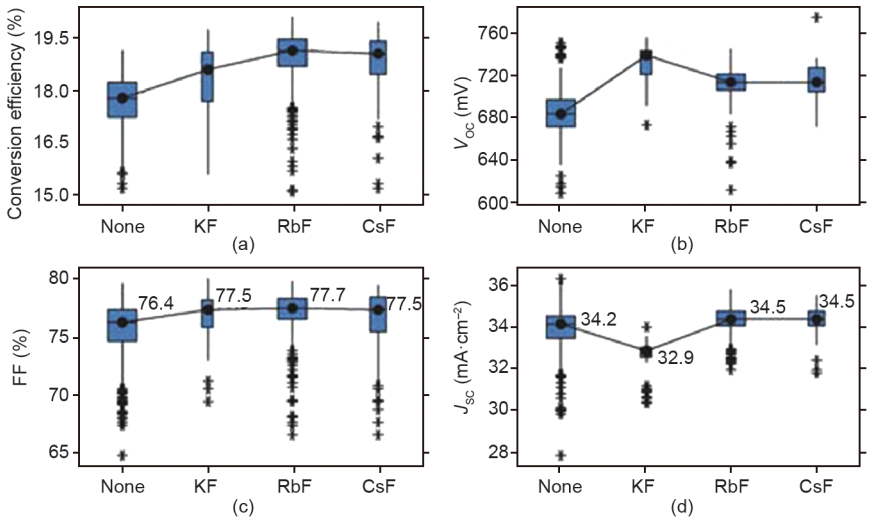

Fig. 6. A comparison of CIGS device parameters with and without alkali PDT [2]. (a) Conversion efficiency; (b) V_{OC}; (c) FF; (d) J_{SC}.

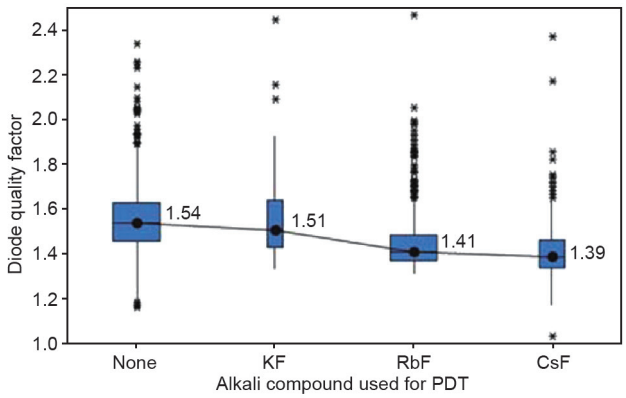

Fig. 7. A comparison of CIGS diode quality factors with and without alkali PDT [2].

heavy alkali element substituted for the doped lighter alkali (Na, K), and that Cs was preferable over Na and K to exist in the CIGS films. At present, the mechanisms of alkali ion exchange and of where the substituted metal atoms (such as depleted Cu and Ga) move are still unclear.

3. Influence of the alkali PDT on CIGS surface and device performance

3.1. J_{SC} improvement with thinner CdS buffer layer

Chirilă et al. [1] analyzed the chemical composition of the CIGS surface with (NaF + KF)-PDT by XPS. It was revealed that Na was substituted by K, while Cu and Ga were depleted within less than 30 nm

Table 4
A comparison of the photovoltaic parameters of CIGS cells with and without alkali PDT.

Sample	Conversion efficiency (%)	V_{OC} (mV)	J_{SC} (mA·cm^{-2})	FF (%)
CsF 320	15.78	670	30.9	76.33
CsF 290	15.44	646	32.0	74.63
CsF 260	15.19	634	32.1	74.63
CsF 0	11.43	550	32.6	63.71

The numbers in the sample names are CsF evaporation temperatures, where CsF 0 stands for "no PDT."

depth at the CIGS surface. Thus, the acceptor defect (V_{Cu}^{-}) density increased in the original ordered vacancy compound (OVC) region of the CIGS surface. During the deposition of CdS film by chemical bath deposition (CBD), the cadmium (Cd) ions diffused to a certain extent into the surface of the absorber material to occupy the V_{Cu}^{-} accepters and form Cd_{Cu} donors. As the donor density was higher than that of the sample with no PDT, the surface inversion was more intense, and thus strengthened the buried homojunction. Therefore, it was not necessary to use a thick buffer layer to form a high-quality CIGS/CdS heterojunction. In addition, for samples with KF-PDT, the CdS layer presented good coverage and uniformity at an early stage of CBD (Fig. 10) [15], so the CdS film could be thinner, which benefited the short wavelength absorption and thus increased the J_{SC}.

3.2. Increased hole concentration at the near-surface of the CIGS

In 2014, Pianezzi et al. [9] prepared CIGS absorber layers on PI

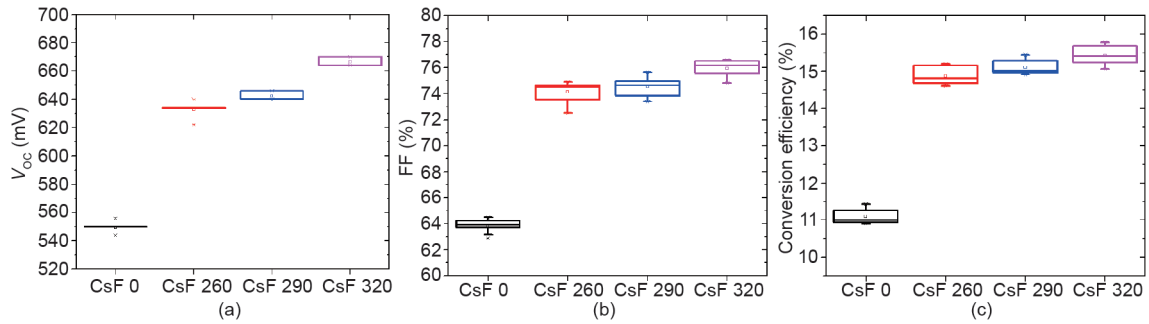

Fig. 8. The effects of CsF doping level on CIGS device output parameters. (a) V_{OC}; (b) FF; (c) conversion efficiency.

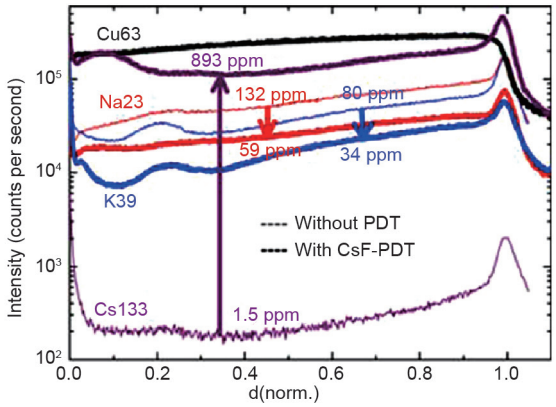

Fig. 9. A SIMS analysis of the K and Na variation in the absorbers without and with CsF-PDT [2]. d(norm.): the sputtering depth, which is normalized by dividing by the whole film thickness.

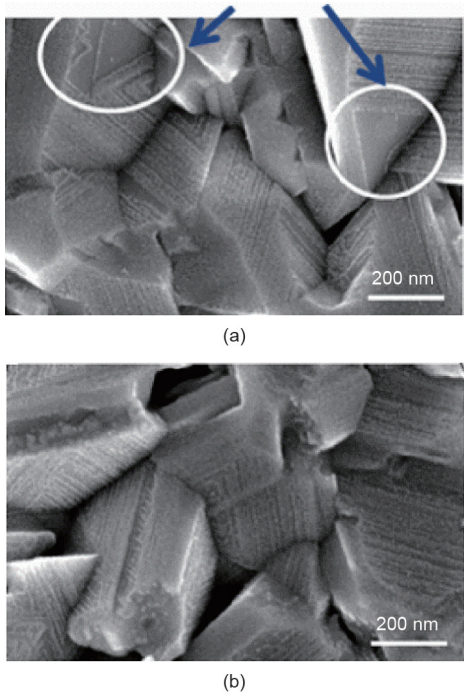

Fig. 10. PDT samples show good coverage in the early stage of CdS deposition [15]. (a) Without PDT; (b) with PDT.

substrates using the three-stage co-evaporation process. Capacitance-voltage (C-V) measurement was applied to characterize the hole concentration of the CIGS absorbers with NaF-PDT, KF-PDT, (NaF + KF)-PDT, and no PDT (Fig. 11). The results show that for the PDT samples, the hole carrier concentration at the CIGS near-surface increased significantly compared with the no-PDT sample. The carrier concentration of the NaF-PDT sample is half an order of magnitude higher than that of the (NaF + KF)-PDT sample, which has a carrier concentration that is slighter higher than that of the KF-PDT sample.

The CIGS absorber surfaces of high-efficiency cells are composed of OVC. A large amount of shallow acceptor defects (V_{Cu}^{-}) and donor defects (In_{Cu}^{2+}) form neutral defect pairs ($2V_{Cu}^{-} + In_{Cu}^{2+}$), and NaF-PDT is able to decompose ($V_{Cu}^{-} + In_{Cu}^{2+}$) defect pairs. Na replaces the donor defects (In_{Cu}^{2+}) to form neutral defects (Na_{Cu}) in In-rich film, and thus improves the hole carrier concentration in the CIGS layers. Na can also occupy the In vacancy (V_{In}) to form the acceptor defect (Na_{In}^{2-}), which is shallower than the Cu_{In}^{2-} acceptor; thus, it further improves the absorber hole concentration. In addition, Na^{+} at the film surface

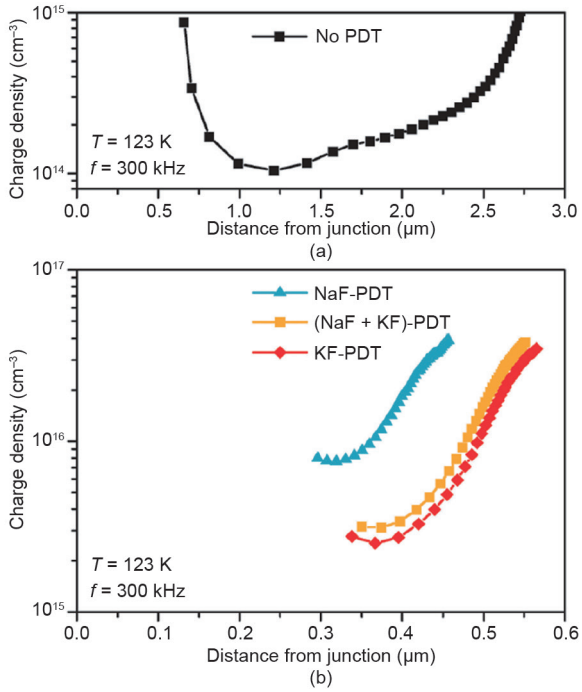

Fig. 11. Hole concentration profiles obtained by C-V measurements. (a) Sample without PDT; (b) samples with NaF-PDT, (NaF + KF)-PDT, and KF-PDT.

will absorb O_2 to transform Se vacancy (V_{Se}) into O_{Se} (Se substituted by O), and will reduce the compensating donor concentration. In general, Na increases the hole concentration in the films for many reasons.

3.3. Wider surface bandgap and lower valance band

Handick et al. [16] provided a depth-dependent band structure measurement at the surface of CIGS absorbers deposited on PI substrates by using ultraviolet photoelectron spectroscopy (UPS), synchrotron-based hard X-ray photoelectron spectroscopy (HAXPES), and inverse photoelectron spectroscopy (IPES). The UPS spectra (He I excited, 21.22 eV) are the most surface sensitive, with an inelastic mean free path (IMFP) of approximately 0.6 nm. By using excitation energies of 2 keV and 8 keV, the values of the IMFP for the HAXPES measurements were increased to 4 nm and 12 nm, respectively. According to the above measurements, three different values of the absorber surface valence band maximum (VBM) were derived. IPES can be used to determine the conduction band minimum (CBM). In Fig. 12 [16], the near-surface bandgap for the NaF-PDT sample was 1.61 eV (+0.14/−0.51 eV). For the (NaF + KF)-PDT CIGS sample, the near-surface bandgap was 2.52 eV (+0.14/−0.51 eV), with the VBM showing a pronounced downward shift from the E_F. Fig. 13 shows the bandgap structure diagram that was calculated according to these experimental data.

Handick et al. [16] proposed that the enlargement of the bandgap at the surface was due to the composition change, which varied the electrical structures. The characterization demonstrated that the surface region was mainly composed of K, In, and Se, and that the bandgap of the In_2Se_3 compound was pronouncedly thickness dependent—that is, the bandgap exceeded 2.5 eV when the thickness decreased to 2.6 μm. The bandgap of $KInSe_2$ was 2.7 eV. It is not possible to distinguish which compound it is, based on the current bandgap data. The two compounds may co-exist, but the ratio is not known yet.

Derived from the data of Fig. 12 [16], the bandgap diagrams of the CIGS/CdS heterojunction with NaF-PDT and (NaF + KF)-PDT are

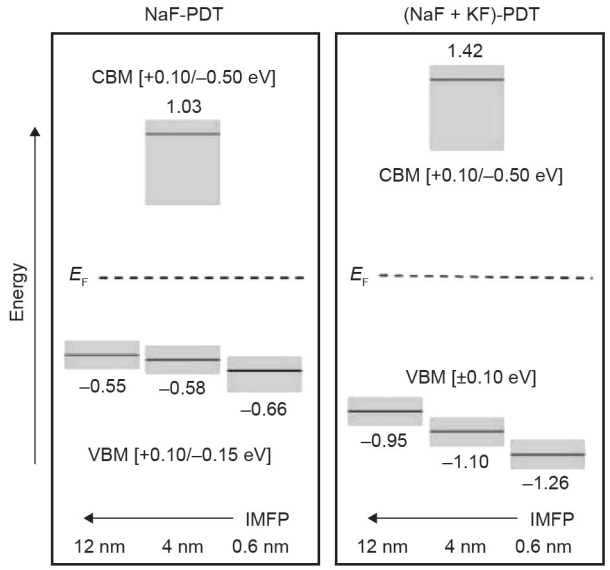

Fig. 12. A bandgap illustration of the near-surface CIGS film with NaF-PDT and (NaF + KF)-PDT [16].

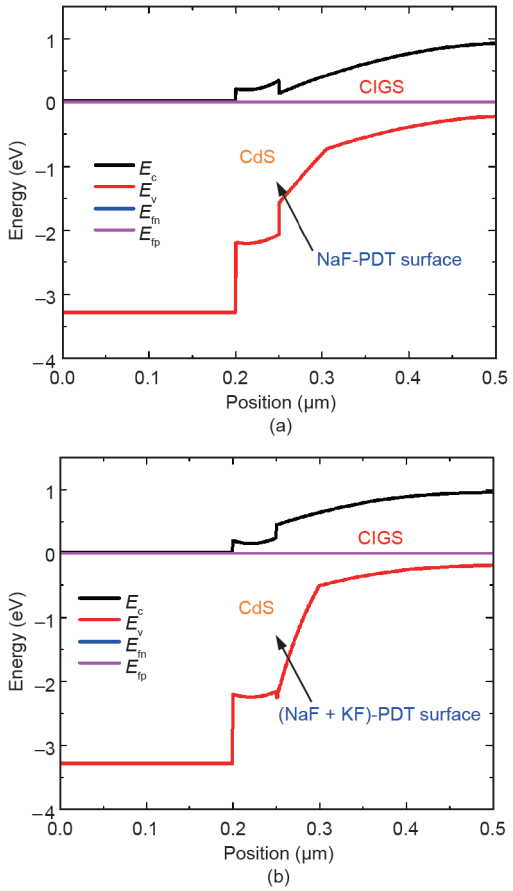

Fig. 13. Bandgap diagram at the CIGS/CdS heterojunction with alkali PDT. (a) NaF-PDT CIGS/CdS; (b) (NaF + KF)-PDT CIGS/CdS. E_c: energy level of minimum of conduction band; E_v: energy level of maximum of valance band; E_{fn}: quasi-Fermi-level of electron; E_{fp}: quasi-Fermi-level of hole.

shown in Fig. 13. The p/n inversion of the CIGS/CdS heterojunction has entered the near-surface region of the CIGS. Holes become the minority carrier at the interface, and the hole concentration determines the magnitude of the interface recombination. As shown in Fig. 13, the VBM of the (NaF + KF)-PDT sample is noticeably shifted downward, more than that of the NaF-PDT CIGS, and the hole concentration is decreased to a great extent. The interface recombination is decreased further, and the V_{OC} and conversion efficiency are obviously improved.

4. Conclusions

In the semiconductor industry, the use of the alkali element Na is a major issue that affects device stability and leads to device failures. Its contamination of silicon wafers must be strictly controlled. In the 1990s, researchers discovered that the alkali element Na could improve the efficiency of CIGS-based solar cells without negative effects on device stability, and re-recognized the mechanisms of how Na acts on multiple compound semiconductor devices. CIGS is a quaternary polycrystalline compound with a conductive mechanism that is totally different from those of elemental semiconductors such as Si and Ge. The conductive type of acceptor or donor depends on the defect structures arising in non-stoichiometry. Alkali elements can change the defect structures via an ion exchange mechanism that is induced by the ion element electronegativity, resulting in the transition of the conductive type. In general, the carrier concentration of the absorber layer can increase, no matter how the alkali element is doped. However, different doping methods will affect the polycrystalline structures of the absorber layer and influence the efficiency.

Alkali PDT can passivate lattice defects without changing the structure of CIGS, and can reduce the diode quality factor and the reverse saturation current so as to improve device performance. Moreover, it has a wide tolerance for the doping amount of the alkali element, especially for the heavy alkali elements, thus contributing to surface structure improvement without changing the CIGS lattice structure. The lower electronegativity of the heavy alkali elements changes the stoichiometry at the CIGS surface, increases the concentration of the acceptor defect (V_{Cu}^-), causes more Cd ions to fill in the acceptor defects (V_{Cu}^-), and increases the concentration of the donor defect (Cd_{Cu}^+). The surface electrical inversion is stronger, and strengthening the buried homojunction at the CIGS surface. In addition, heavy alkali PDT improves the CdS coverage, allowing the CdS to be thinner in order to increase the short wavelength absorption. This is an important factor in increasing device efficiency. Heavy alkali PDT also broadens the CIGS surface bandgap and lowers the valence band maximum of the CIGS surface, while the lower hole concentration further suppresses carrier recombination at the interface. This is another important reason for the improvements in V_{OC} and conversion efficiency.

The use of heavy alkali PDT has resulted in breakthrough progress for CIGS-based solar cells, and significantly decreases the efficiency gap between thin-film solar cells and single crystalline silicon-based solar cells. The European Union's Sharc25 project (super high-efficiency Cu(In,Ga)Se_2 thin-film solar cells approaching 25%) demonstrates that the CIGS surface and interface characteristics have a major impact on improving cell efficiency up to 25%; therefore, more innovations and developments in this field are expected in the near future.

Acknowledgements

This work is supported by the YangFan Innovative & Entrepreneurial Research Team Project (2014YT02N037).

Compliance with ethics guidelines

Yun Sun, Shuping Lin, Wei Li, Shiqing Cheng, Yunxiang Zhang, Yiming Liu, and Wei Liu declare that they have no conflict of interest or financial conflicts to disclose.

References

[1] Chirilă A, Reinhard P, Pianezzi F, Bloesch P, Uhl AR, Fella C, et al. Potassium-induced surface modification of $Cu(In,Ga)Se_2$ thin films for high-efficiency solar cells. Nat Mater 2013;12(12):1107–11.

[2] Jackson P, Wuerz R, Hariskos D, Lotter E, Witte W, Powalla M. Effects of heavy alkali elements in $Cu(In,Ga)Se_2$ solar cells with efficiencies up to 22.6%. Phys Status Solidi–R 2016;10(8):583–6.

[3] Hedström J, Ohlsen H, Bodegård M, Kylner A, Stolt L, Hariskos D, et al. ZnO/CdS/$Cu(In,Ga)Se_2$ thin film solar cells with improved performance. In: Proceedings of the 23rd IEEE Photovoltaic Specialists Conference; 1993 May 10–14; Louisville, KY, USA. Piscataway: The Institute of Electrical and Electronics Engineers, Inc.; 1993. p. 364–71.

[4] Bodegård M, Stolt L, Hedström J. The influence of sodium on the grain structure of $CuInSe_2$ films for photovoltaic applications. In: Hill R, Palz W, Helm P, editors Twelfth European Photovoltaic Solar Energy Conference: Proceedings of the international conference; 1994 Apr 11–15; Amsterdam, the Netherlands. London: James & James (Science Publishers) Ltd.; 1994. p. 1743–6.

[5] Holz J, Karg F, von Philipsborn H. The effect of substrate impurities on the electronic conductivity in CIS thin films. In: Hill R, Palz W, Helm P, editors Twelfth European Photovoltaic Solar Energy Conference: Proceedings of the international conference; 1994 Apr 11–15; Amsterdam, the Netherlands. London: James & James (Science Publishers) Ltd.; 1994. p. 1592–5.

[6] Granata JE, Sites JR, Asher S, Matson RJ. Quantitative incorporation of sodium in $CuInSe_2$ and $Cu(In,Ga)Se_2$ photovoltaic devices. In: Proceedings of the 26th IEEE Photovoltaic Specialists Conference; 1997 Sep 29–Oct 3; Anaheim, CA, USA. Piscataway: The Institute of Electrical and Electronics Engineers, Inc.; 1997. p. 387–90.

[7] Contreras MA, Egaas B, Dippo P, Webb J, Granata J, Ramanathan K, et al. On the role of Na and modifications to $Cu(In,Ga)Se_2$ absorber materials using thin-MF (M = Na, K, Cs) precursor layers. In: Proceedings of the 26th IEEE Photovoltaic Specialists Conference; 1997 Sep 29–Oct 3; Anaheim, CA, USA. Piscataway: The Institute of Electrical and Electronics Engineers, Inc.; 1997. p. 359–62.

[8] Rudmann D, Brémaud D, Zogg H, Tiwari AN. Na incorporation into $Cu(In,Ga)Se_2$ for high-efficiency flexible solar cells on polymer foils. J Appl Phys 2005;97(8):084903.

[9] Pianezzi F, Reinhard P, Chirilă A, Bissig B, Nishiwaki S, Buecheler S, et al. Unveiling the effects of post-deposition treatment with different alkaline elements on the electronic properties of CIGS thin film solar cells. Phys Chem Chem Phys 2014;16(19):8843–51.

[10] Laemmle A, Wuerz R, Schwarz T, Cojocaru-Mirédin O, Choi PP, Powalla M. Investigation of the diffusion behavior of sodium in $Cu(In,Ga)Se_2$ layers. J Appl Phys 2014;115(15):154501.

[11] Caballero R, Kaufmann CA, Eisenbarth T, Unold T, Klenk R, Schock HW. High efficiency low temperature grown $Cu(In,Ga)Se_2$ thin film solar cells on flexible substrates using NaF precursor layers. Prog Photovoltaics 2011;19(5):547–51.

[12] Salomé P, Fjällström V, Hultqvist A, Edoff M. Na doping of CIGS solar cells using low sodium-doped Mo layer. IEEE J Photovolt 2013;3(1):509–13.

[13] Güttler D, Chirila A, Seyrling S, Blösch P, Buecheler S, Fontané X, et al. Influence of NaF incorporation during $Cu(In,Ga)Se_2$ growth on microstructure and photovoltaic performance. In: Proceedings of the 35th IEEE Photovoltaic Specialists Conference; 2010 Jun 20–25; Honolulu, HI, USA. Piscataway: The Institute of Electrical and Electronics Engineers, Inc.; 2010. p. 3420–4.

[14] Brummer A, Honkimäki V, Berwian P, Probst V, Palm J, Hock R. Formaton of $CuInSe_2$ by the annealing of stacked elemental layers—Analysis by *in situ* high-energy powder diffraction. Thin Solid Films 2003;437(1–2):297–307.

[15] Paetel S. Roadmap CIGS towards 25% efficiency [presentation]. In: 7th International Workshop on CIGS Solar Cell Technology; 2016 Jun 23; Munich, Germany; 2016.

[16] Handick E, Reinhard P, Alsmeier JH, Köhler L, Pianezzi F, Krause S, et al. Potassium postdeposition treatment-induced band gap widening at $Cu(In,Ga)Se_2$ surfaces—Reason for performance leap? ACS Appl Mater Interfaces 2015;7(49):27414–20.